Available online at www.sciencedirect.com
ScienceDirect
Polymer 48 (2007) 3349–3360
polymer
www.elsevier.com/locate/polymer

Constitutive modeling of HDPE polymer/clay nanocomposite foams

Choonghee Jo [a], Hani E. Naguib [b,*]

[a] Department of Mechanical Engineering, University of Ottawa, Ottawa, ON, Canada K1N 6N5
[b] Department of Mechanical and Industrial Engineering, University of Toronto, 5 King's College Road, Toronto, ON, Canada M5S 3G8

Received 26 September 2006; received in revised form 17 March 2007; accepted 19 March 2007
Available online 30 March 2007

Abstract

A constitutive model for tensile behavior of high density polyethylene (HDPE)/clay nanocomposite foams was proposed. The elastic modulus of HDPE/clay nanocomposite was developed using micromechanics theory, and the modulus for foams was obtained by using representative volume element (RVE) concept. In order to describe the tensile behavior of the foams, a constitutive equation obtained from a viscoelastic model was proposed. The constitutive model was expressed in terms of microstructural properties of polymer, and physical properties of the foams. The effects of the material parameters and processing conditions on the foam morphologies and mechanical properties of HDPE/clay nanocomposite foams were investigated. Microcellular closed-cell nanocomposite foams were manufactured with HDPE, where the nanoclay loadings of 0.5, 1.0, and 2.0 wt% were used. The effect of clay loading and foaming conditions on the volume expansion ratio, elastic modulus, tensile strength, and elongation at break was investigated. Except for the elongation at break, the mechanical properties were improved with nanoclay loading. The tensile experimental data of the foams were compared with the prediction by the theoretical model. It was demonstrated that the tensile behaviors of HDPE/clay nanocomposite foams were well described by the constitutive model.

Keywords: Constitutive equation; HDPE; Nanocomposite foams

1. Introduction

Polymer/clay nanocomposites are of interest because the characteristics of nanometer scaled silicate pellets, such as high aspect ratio and their nanometer scale dispersibility, contribute to a good reinforcement and improve the mechanical properties of the polymer [1,2]. Also, nanocomposites generally provide improvements in transport barrier, thermal resistivity, and flame-retardance in comparison with the original polymers [3–5].

Also, recently, a great deal of interest has been focused on the polymer/clay nanocomposite foams. Since the size of the filler is in the order of nanometers, it can be used as a nucleation agent in microcellular polymeric foam processing [6]. Nanofillers have at least one dimension in the order of 1 nm and the platelet-shaped nanofillers have high aspect ratios from 10 to 1000 [1]. The interfaces between the nanofillers and the polymer are potential nucleation sites where heterogeneous nucleation can be induced. Microcellular foams usually have average cell sizes from 0.1 μm to 10 μm, and cell densities in the range of 10^9–10^{15} cells/cm^3 [7]. The mechanical properties of microcellular foams have been of great interest because of their unique microstructure. Compared to the unfoamed polymer, microcellular foams generally possess superior properties such as higher strength-to-weight ratio [8], higher impact strength [9,10], increased toughness [11], prolonged fatigue life [12] and an increased thermal stability, and increased thermal and electrical insulation properties [13,14]. Therefore, microcellular foams have a great potential for applications such as packaging, insulation, automotive and aircraft industries, and structural components. In addition, microcellular plastics are produced using environmentally safe gases such as nitrogen and carbon dioxide.

Accordingly, studies for characterizing the properties of polymer/clay nanocomposites and their foams are increasing.

* Corresponding author. Tel.: +1 416 978 7054; fax: +1 416 978 7753.
E-mail address: naguib@mie.utoronto.ca (H.E. Naguib).

0032-3861/$ - see front matter © 2007 Elsevier Ltd. All rights reserved.
doi:10.1016/j.polymer.2007.03.056

Also, as the use of semicrystalline polymer/clay nanocomposite foams is increased, there is an emerging need for the study of the constitutive models for the foams as well as for the nanocomposites. Generally, the elastic modulus of polymer/clay composites increases with augmenting the clay volume fractions, while the yield stress and strain decrease with increasing clay volume fraction [15,16]. The enhancing effect of clay in HDPE applies mainly to the modulus rather than the strength [17]. This enhancing phenomenon is due to the exfoliation of the clays in the matrix and high aspect ratio of clay particles. Lee and Paul [18] developed a model for the mechanical properties of a nanocomposite containing complex inclusions by using the Eshelby's equivalent tensor with a Mori–Tanaka type model. This model permits predictions for sphere, disc, and fiber shaped inclusions, and the influences of the primary and secondary aspect ratios on the effective elastic moduli were examined. However, it is limited to unidirectionally aligned inclusions. The effect of the nanoparticles on the elastic modulus of polymer/clay nanocomposites has been studied experimentally [19–24]. Some micromechanically-based constitutive models for semicrystalline polymers have been studied [25–27]. Also, a multi-scale modeling strategy considering the hierarchical morphology of the polymer/nanocomposite was developed by Sheng et al. [28]. In the case of using HDPE, Nikolov et al. [29] proposed a multi-scale constitutive model for small deformations of semicrystalline polymers, where viscoelastic and viscoplastic models were used for crystalline lamellae and amorphous phase behavior, respectively.

Studies on the influence of the nanoparticles on the constitutive modeling of semicrystalline polymer nanocomposites are increasing. However, only few models for HDPE/clay nanocomposites have been reported [15,17,19,28,30]. Moreover, little study has been performed for the constitutive modeling of the polymer/clay nanocomposite foams. A constitutive model is derived for the viscoplastic response of polyethylene/montmorillonite clay nanocomposite at three-dimensional cyclic deformations with small strains [30]. The study focuses on low-cycle deformation. Luo and Daniel [19] developed a three-phase model including the epoxy matrix, the exfoliated clay nanolayers and the nanolayer clusters. In the model, the region consisting of matrix with exfoliated clay nanolayers or platelets is analyzed by assuming near uniform dispersion and random orientation. The properties of intercalated clusters of clay platelets are calculated by a rule of mixtures based on a parallel platelet system. The Mori–Tanaka method is applied to calculate the modulus of the nanocomposite as a function of various parameters, including the exfoliation ratio, clay layer and cluster aspect ratios, *d*-spacing, intragallery modulus, matrix modulus and matrix Poisson's ratio. When HDPE is melt compounded with an organically modified montmorillonite, the composite film involves intercalated clay particles, where the clay enhancing effects apply mainly to the modulus, instead of the strength [17]. Also, the influence of the organic monolayer structure on the exfoliation of montmorillonite and the tensile properties of the HDPE/organo-montmorillonite nanocomposites was studied [15]. The tensile properties were correlated to the volume fraction of the inorganic part of the nanocomposites. A multi-scale modeling strategy was employed to account for the hierarchical morphology of the nanocomposite [28]. These geometric features of clays together with estimates of silica lamina stiffness provide a basis for modeling effective mechanical properties of the clay particle. In the case of the semicrystalline matrices, the transcrystallization behavior induced by the nanoclay is taken into account by modeling a layer of matrix surrounding the particle to be highly textured and therefore mechanically anisotropic.

In the present paper, a constitutive model for estimating the tensile behavior of HDPE/clay nanocomposite foams was proposed. A model for elastic modulus of HDPE/clay nanocomposite foams was developed by using micromechanics (representative volume element (RVE)) concept. The difference in the modeling of elastic modulus between the current work using HDPE/clay nanocomposites and the previous work [31] using PMMA/clay nanocomposites is on the type of clay dispersion in the polymer matrix. In the case of PMMA/clay nanocomposite foams, both deteriorating effect by agglomerated clays and enhancing effect by intercalated clays on the elastic modulus were considered. However, in the present work, only intercalated clay model was used because, within the used wt% clay concentration, the overall elastic modulus is not decreased but increases very slowly as the clay content increases. Thus, the intercalated clay stacks in HDPE/clay nanocomposites are modeled so that the rate of enhancing effect on the modulus is diminished gradually. In order to describe the tensile elastic behavior of the foams, a viscoelastic model was used. The constitutive model was expressed in terms of microstructural properties of polymer and physical properties of the foams. Also, the effects of the material parameters and processing conditions on the foam morphologies and mechanical properties of HDPE/clay nanocomposite foams were investigated. Microcellular HDPE/clay nanocomposite foams were manufactured using a batch processing method with nanoclay loadings of 0.5, 1.0, and 2.0 wt%. Then, the influence of clay loading and foaming conditions on the volume expansion ratio, elastic modulus, tensile strength, and elongation at break was investigated. The tensile experimental data of the foams were compared with the prediction by the theoretical model.

2. Constitutive modeling for HDPE/clay nanocomposite foams

2.1. Elastic modulus of HDPE/clay nanocomposites

A model for elastic modulus of HDPE/clay nanocomposite is proposed using micromechanics theory. On the modeling of the mechanical property of nanocomposites, the effect of the clay particles on the polymer matrix needs to be investigated first. The lamellar thickness and interlamellar spacing of HDPE increased when the crystallization temperature was increased [32]. The crystallization temperatures of HDPE/clay nanocomposites were tested by Lee et al. [33]: as the clay contents vary from 0 to 3 wt% the crystallization temperature

increased from 117.4 to 118.8 °C. At this temperature range, the change in the interlamellar spacing and lamellar thickness was small, keeping 12 nm and 26 nm, respectively [32]. Thereof, in this study, the thicknesses of crystalline and amorphous layers in the HDPE are assumed not to be changed even though clays are added. At low clay loadings, some clay particles are observed as well-dispersed structure throughout the HDPE matrix, and as the clay content increases some clay stacks show an intercalated structure [33]. However, in this study, all clay particles are modeled as intercalated structures for simplicity sake, and at the same time, variable clay spacing depends on the clay contents is considered in the model.

The intercalated clay stacks are modeled as cuboids which have dimensions a_1 and thickness a_3, and one of the length directions always keeps a right angle to the load direction (Fig. 1). When the angle between the clay plane and load direction varies from 0° to 90°, the reinforcing effect of the clays on the elastic modulus can vary from maximum to minimum. If each intercalated clay stack is deformed uniformly both in the length direction (δa_1) and in the thickness direction (δa_3), the displacement of the clay stack in the load direction can be expressed as:

$$u_p = \delta a_3 \cos\theta, \tag{1}$$

where θ is the angle between the clay plane and the plane perpendicular to the load. When an overall tensile stress (σ) is applied in a RVE, the force applied on a clay stack becomes $\sigma a_1^2 \cos\theta$. Since the force component to the direction of clay thickness is $\sigma a_1^2 \cos^2\theta$, the displacement δa_3 is calculated from the linear stress–strain relationship, as:

$$\delta a_3 = \frac{\sigma a_3 \cos^2\theta}{E_R}, \tag{2}$$

where E_R is the elastic modulus for the laminated composite by the Reuss model ($\theta = 0$). Originally, the Reuss model was made for large-particle composites. However, since the intercalated clay stacks have a dimension greater than 100 nm, the Reuss model does apply in this model. Inserting Eq. (2) into Eq. (1) u_p is obtained as:

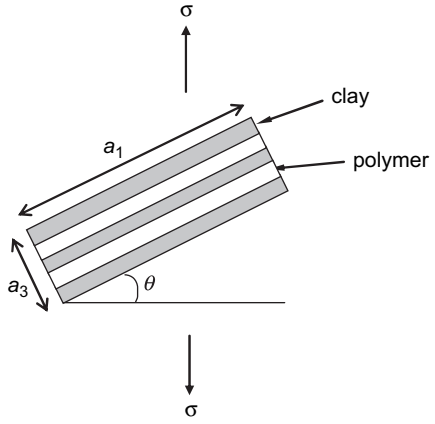

Fig. 1. Model for intercalated clay stack.

$$u_p = \frac{\sigma a_3 \cos^3\theta}{E_R}. \tag{3}$$

In the case of no clays, the corresponding displacement in the direction of load is

$$u_0 = \frac{\sigma a_3}{E_m \cos\theta}, \tag{4}$$

where E_m is the elastic modulus of polymer matrix. Thus, the decrease of the tensile displacement of an intercalated clay stack due to the presence of the clay is:

$$u = u_0 - u_p = \frac{\sigma a_3}{\cos\theta}\left(\frac{1}{E_m} - \frac{\cos^4\theta}{E_R}\right). \tag{5}$$

The decreased overall strain due to a clay stack can be obtained by using the RVE concept as:

$$\bar{\varepsilon}^{\alpha} = \frac{1}{V}\frac{2}{\pi}\int_0^{\pi/2} u a_1^2 \cos\theta \, d\theta = \frac{a_1^2 a_3}{V}\sigma\left(\frac{1}{E_m} - \frac{3}{8E_R}\right). \tag{6}$$

In Eq. (6), $a_1^2 a_3 V^{-1}$ is the volume fraction of the intercalated clay region and can be expressed using the volume fraction of clay particles (v_p) as [31]:

$$v_{pi} = v_p\left(1 + \frac{n_p - 1}{n_p}\frac{d_m}{d_p}\right), \tag{7}$$

where n_p is the number of clay layers in each intercalated clay stack, d_p and d_m are the clay layer thickness and clay layer spacing, respectively. Then, the overall strain decreased by all intercalated clay stacks are:

$$\bar{\varepsilon}^{p} = N\bar{\varepsilon}^{\alpha} = v_{pi}\sigma\left(\frac{1}{E_m} - \frac{3}{8E_R}\right). \tag{8}$$

Thus, the effective strain becomes $\bar{\varepsilon} = \varepsilon^0 - \bar{\varepsilon}^p$ and by using $\varepsilon^0 = \sigma/E_m$ and $E_R = (E_m E_p)[E_m v_{pi} + E_p(1 - v_{pi})]^{-1}$, the effective elastic modulus of HDPE/clay nanocomposites is yielded as:

$$\bar{E} = E_m'\left\{1 - v_{pi} + \frac{3v_{pi}}{8E_p}[E_p - v_{pi}(E_p - E_m')]\right\}^{-1}, \tag{9}$$

in which E_m' is the elastic modulus of HDPE containing PE-*g*-MAn. When PE-*g*-MAn is added to the HDPE the elastic modulus increased by 4% compared to the pure HDPE [34]. In Eq. (9), the modulus of the volume between the clay layers is assumed to have the same modulus as clay layers. The macromolecular chains intercalated in clay layers are confined in a very small space and their behavior is quite different from those in bulk matrix, which results in macromolecules becoming rigid [35–37]. Also, the increasing effect of the tensile modulus by considering the interfacial region between the polymer matrix and clay particles was proved by Ji et al. [37]. Therefore, the elastic modulus in the intercalated region can usually be regarded as the same to that of clay particles.

2.2. Elastic modulus of HDPE/clay nanocomposite foams

Since most HDPE/clay nanocomposite foams have relatively low volume expansion ratios [33,38,39], the following two conditions can be considered in the modeling of the elastic modulus: there is a dilute distribution of the voids in the polymer matrix and the voids are randomly distributed. In this study, the shape of voids in the foams is assumed as spherical cavities. Under the uniaxial tensile loading, the cavities in RVE cause an increase of the tensile strain. Thus, the overall strain increment of the polymer nanocomposites containing voids can be estimated from the locally incremented strains. Within the volume V of RVE, the average strain ($\bar{\varepsilon}$) is expressed as:

$$\bar{\varepsilon} = \bar{\varepsilon}^0 + \bar{\varepsilon}^c, \tag{10}$$

where $\bar{\varepsilon}^0$ is the average strain of the RVE without cavities and $\bar{\varepsilon}^c$ is the additional strain increment due to the presence of the cavities. The magnitude of $\bar{\varepsilon}^c$ can be obtained by using the virtual stress–strain concept on the cavity surfaces and reciprocal theorem [40] as:

$$\bar{\varepsilon}^c = \frac{1}{V}\int_{\partial\Omega} \frac{1}{2}(n\otimes u + u\otimes n)\mathrm{d}S, \tag{11}$$

where $\partial\Omega$ denotes cavity surface and n is the exterior unit normal on the cavity surface and u is the displacement by actual loading. When the coordinate axes are formed at the center of a spherical cavity of radius R, the displacement field in the infinite elastic body under uniaxial remote tension (σ) was derived within the linear elastic theory [41] as:

$$u_r = \frac{\sigma r}{4\mu}\left[\frac{2+\Lambda}{2+3\Lambda} + \frac{13+8\Lambda}{14+9\Lambda}\left(\frac{R}{r}\right)^3 - \frac{3(1+\Lambda)}{14+9\Lambda}\left(\frac{R}{r}\right)^5\right] + \frac{\sigma r}{4\mu}\left[1 + \frac{5(5+3\Lambda)}{14+9\Lambda}\left(\frac{R}{r}\right)^3 - \frac{9(1+\Lambda)}{14+9\Lambda}\left(\frac{R}{r}\right)^5\right]\cos 2\theta, \tag{12}$$

where r is the radial distance in the spherical coordinate and θ is the angle from the tensile loading axis. The parameter Λ is expressed as $\Lambda = \lambda/\mu$, where λ is a Ramé constant and μ is the shear modulus. The radial displacement at the surface of the spherical cavity is obtained from Eq. (12), where $\Lambda = 2\nu/(1-2\nu)$ was used:

$$u_R = \frac{3\sigma R(1-\nu)}{\mu(7-5\nu)}\left(\frac{1}{1+\nu} + \frac{5}{4}\cos 2\theta\right), \tag{13}$$

where ν is the Poisson's ratio. The additional overall volumetric strain by a cavity is defined as:

$$\bar{\varepsilon}^R \equiv \frac{1}{V}\int_{\partial\Omega_R} \frac{1}{2}(n\otimes u + u\otimes n)\mathrm{d}S. \tag{14}$$

Thus, $\bar{\varepsilon}^R$ is obtained by substituting u_R into Eq. (14) and integration from $\theta = 0$ to $\theta = \pi$ as:

$$\begin{aligned}\bar{\varepsilon}^R &= \frac{1}{V}\int_{\partial\Omega_R} u_R \mathrm{d}S \\ &= \frac{1}{V}\frac{3\sigma R(1-\nu)}{\mu(7-5\nu)} 2\pi R^2 \left(2\int_0^{\pi/2} \frac{1}{1+\nu}\sin\theta\,\mathrm{d}\theta + 2\int_0^{\pi/2}\frac{5}{4}\cos 2\theta\sin\theta\,\mathrm{d}\theta\right) \\ &= \frac{1}{V}\frac{\pi R^3(1-\nu)}{\mu(1+\nu)}\sigma.\end{aligned} \tag{15}$$

For simplicity sake, when all cavities in RVE are assumed to be uniform and have dilute distribution, then $\bar{\varepsilon}^c = N\bar{\varepsilon}^R$, where N is the total number of cavities per unit volume.

The applicability of dilute distribution and uniform distribution of cavities in this model is verified quantitatively by comparing the stress over the surroundings of the cavity with overall stress. In the dilute distribution of micro-inclusions, the interactions among inclusions are not considered. Also, the inclusions are assumed to be distributed evenly throughout the volume. In this situation, elastic moduli do not depend on the distance between inclusions [42]. When the overall stresses are assumed to be prescribed, it underestimates the effect of the interaction between cracks [43]. However, prescribed stress is not considered in this model. First, the distance between cells in the foams is calculated with the following model. If the voids in the foams are assumed as spherical cavities and densely packed in a cube, a packing model of the spheres in the cube can be proposed. When the diameter of spheres and the dimension of cube are D and $d(=n\times D)$, respectively, n spheres are arrayed along one edge of the cube. Then, another array is added at the next of the first array so that each of the spheres can be located between the spheres in first array, where the distance between the first array and the second array is calculated as $(\sqrt{3}/2)D$. So, $(2/\sqrt{3})$ arrays are located on the other side of cube. Now, $n\times(2/\sqrt{3})n$ spheres are packed on a plane. Next, the same plane arrays are placed on top of the first plane array so that each of the spheres in the second plane can be positioned at the center of the three spheres in the first plane. Then, the distance between planes is $(3/4)D$. Therefore, the total number of spheres packed in the cube becomes $n\times(2/\sqrt{3})n\times(4/3)n = (8/3\sqrt{3})n^3$. This packing model can be an example of the distribution of cells in the foams which have uniform distance among cells. In this case, the distance among cells is equal to D because all adjacent spheres are contacted at the surface of the sphere and the center of cells is coinciding with the center of the spheres. In this model, the size of cells should be smaller than the spheres and is assumed to have diameter D'. Then, the volume of cells in the foam is expressed as $(4\pi)(D'/D)^3 d^3/(9\sqrt{3})$, where $n = d/D$ was used. The volume ratio of air in the cube foam is $(4\pi)(D'/D)^3/(9\sqrt{3})$, and is equal to $(1-1/E_R)$, where E_R is the volume expansion ratio of foams. Therefore, the ratio of the distance between cells

and cell diameter is represented as a function of volume expansion ratio as:

$$\frac{D}{D'} = \left[\frac{9\sqrt{3}}{4\pi}\left(1 - \frac{1}{E_R}\right)\right]^{-1/3}, \tag{16}$$

and plotted in Fig. 2. In the range of the volume expansion ratio from 1.02 to 1.07, the ratios of the distance between cells and cell diameter were 2.5–3.5. Next, the influence of stresses due to a cavity over the surroundings of the cavity is investigated. When an external remote tension load is applied at infinity, the tangential component of the stress at cavity is expressed as [44]:

$$\sigma_\theta = \frac{\sigma_0}{2}(1 - \cos 2\theta) + \sigma_0\left\{\frac{13}{4(7-5\nu)}\left(\frac{R}{r}\right)^3 - \frac{3}{4(7-5\nu)}\left(\frac{R}{r}\right)^5 + \left[\frac{5(1-2\nu)}{4(7-5\nu)}\left(\frac{R}{r}\right)^3 - \frac{21}{4(7-5\nu)}\left(\frac{R}{r}\right)^5\right]\cos 2\theta\right\}, \tag{17}$$

where R is the radius of cavity, r is the radial distance from the center of cavity, and ν is Poisson's ratio. To investigate the effect of this stress on other cavities, the magnitude of this stress in the direction of applied load ($\theta = \pi/2$) is calculated between cavities. As shown in Fig. 3, this stress is maximum at the surface of the cavity and decreases as r increases. Since the influence of this stress is almost disappeared at the distances longer than 2.5 times of the cavity radius, the interactions between cells can be negligible in the r/R range between 2.5 and 3.5. Thus, the distribution of cells in HDPE/clay nanocomposite foams can be regarded as a dilute distribution because the interactions among cells may not be considered.

Therefore, the additional volumetric strain due to the presence of the cavities can be expressed by:

$$\overline{\varepsilon}^c = f\frac{3(1-\nu)}{4\mu(1+\nu)}\sigma, \tag{18}$$

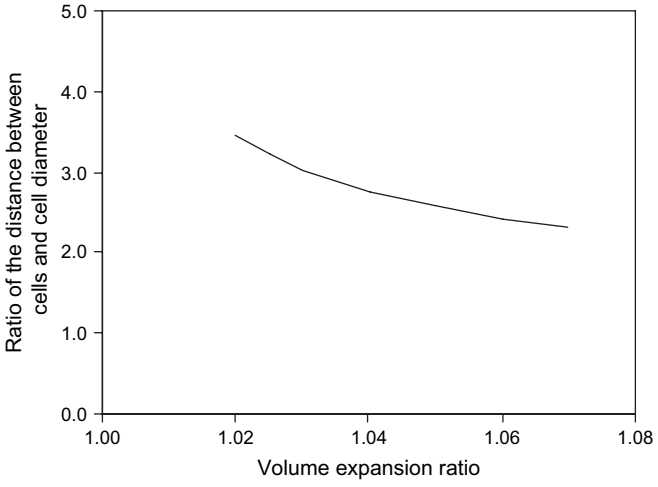

Fig. 2. The ratio of the distance between cells and cell diameter represented as a function of volume expansion ratio.

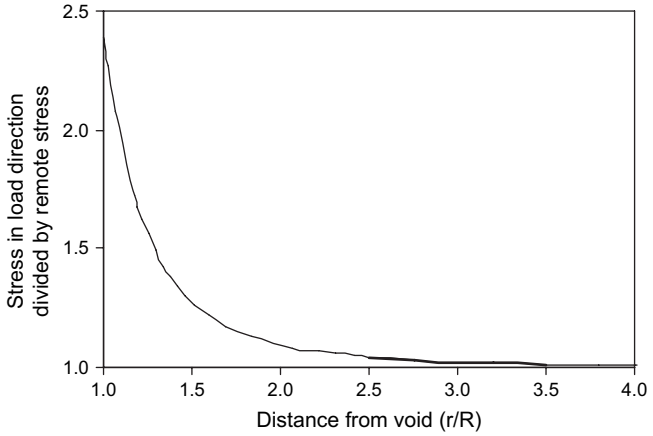

Fig. 3. Stress concentration factor in load direction between cells.

where f is the volume fraction of the cavities in RVE. The additional volumetric strain in Eq. (18) is sum of the component in the direction of uniaxial tensile stress and the component in the other two perpendicular directions. Then, within the isotropic linear elasticity, the component of additional volumetric strain in the direction of tensile stress (σ) is obtained as:

$$\overline{\varepsilon}^c_{xx} = (1-2\nu)\overline{\varepsilon}^c. \tag{19}$$

Thus, the average strain defined in Eq. (10) is modified for the effective strain in the uniaxial stress direction as:

$$\overline{\varepsilon} = \overline{\varepsilon}^0 + \overline{\varepsilon}^c_{xx}. \tag{20}$$

By using $\overline{\varepsilon} = \sigma/\overline{E}$ and $\overline{\varepsilon}^0 = \sigma/E$, Eq. (20) is changed to:

$$\frac{\sigma}{\overline{E}} = \frac{\sigma}{E} + (1-2\nu)f\frac{3(1-\nu)}{4\mu(1+\nu)}\sigma. \tag{21}$$

Then, the overall elastic modulus is expressed as:

$$\overline{E} = \left[\frac{1}{E} + (1-2\nu)f\frac{3(1-\nu)}{4\mu(1+\nu)}\right]^{-1}. \tag{22}$$

If volume fraction of cavities is converted to the relative density of foams (ρ_r) and shear modulus is expressed by elastic modulus, the ratio of elastic modulus of foams ($\overline{E}^*$) and that of unfoamed polymer is yielded as:

$$\frac{\overline{E}^*}{E} = \left[1 - (1-\rho_r)\frac{3(1-\nu)}{2(1-2\nu)}\right]. \tag{23}$$

Eq. (23) is valid at the beginning of the tensile deformation because both unfoamed and foamed materials show linear elastic property at the starting of the deformation. Therefore, replacing E in Eq. (23) with the elastic modulus of HDPE/clay nanocomposites (Eq. (9)), the elastic modulus of foams ($\overline{E}^*$) is yielded as a function of the relative density of foams (ρ_r),

$$\overline{E}^* = E'_m\left\{1 - v_{pi} + \frac{3v_{pi}}{8E_p}[E_p - v_{pi}(E_p - E'_m)]\right\}^{-1} \times \left[1 - (1-\rho_r)\frac{3(1-\nu)}{2(1-2\nu)}\right]. \tag{24}$$

This expression is valid for the foams which have low void fractions.

2.3. Constitutive equation

The tensile behavior of HDPE/clay nanocomposite foams can be described by viscoelastic–plastic constitutive model. For overall behavior of polycrystal structure, a self-consistent approach using large deformation viscoplastic theory was developed by Molinari et al. [45], where elasticity was neglected. Since the amorphous phase plays a predominant role in many aspects of the properties of semicrystalline polymers [46], elastic part of tensile deformation is considered first in the present paper, and viscoplasticity model is left for future study. The mechanism of elastic deformation in response to tensile stress is due to the elongation of the chain molecules in the direction of the applied load. The semicrystalline polymers can be modeled using lamellar crystal layers separated by amorphous layers. Among the deformation mechanisms of amorphous layers of HDPE, interlamellar shear parallel to the lamellae is dominant in the early phase of deformation [47,48]. To describe the overall elastic behavior by shear deformation of amorphous layers, a three-element viscoelastic model (Fig. 4) can be used, where the proposed elastic modulus of foams can be applied directly. The elastic modulus E_1 in Fig. 4 depends on the strain rate [49]. However, it is considered as a constant for simplicity sake because a constant strain rate is used in this study. The equation of motion of the three-element viscoelastic model is:

$$\dot{\sigma}+\frac{E_1}{\eta}\sigma=\frac{E_1E_2}{\eta}\varepsilon+(E_1+E_2)\dot{\varepsilon}. \tag{25}$$

The corresponding constitutive relation is obtained from Eq. (25) as:

$$\sigma=\overline{E}\varepsilon-\frac{\eta}{\tau}\varepsilon+\eta\dot{\varepsilon}\left[1-\exp\left(-\frac{\varepsilon}{\tau\dot{\varepsilon}}\right)\right], \tag{26}$$

where the equivalent elastic modulus ($\overline{E}$) and relaxation time constant (τ) [50] are E_1+E_2 and ηE_1^{-1}, respectively. When Eq. (26) is used for HDPE/clay nanocomposite foams Eq. (24) is substituted for $\overline{E}$. The crystallinity was not used in Eq. (26). However, the influence of crystallinity is controlled indirectly by viscoelastic parameters.

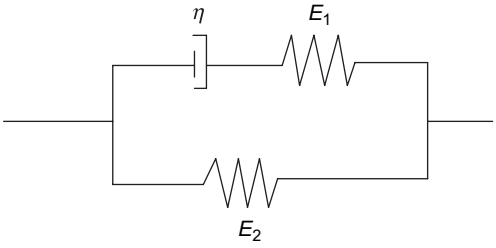

Fig. 4. Three-element viscoelastic model.

3. Experimentation

Microcellular HDPE/clay nanocomposite foams were manufactured in a batch processing method and their mechanical properties were obtained by experiment.

3.1. Materials

HDPE (SCLAIR 59A, Nova Chemicals) with a density of 0.962 (ASTM D792) and a melt index of 0.72 g/10 min (ASTM D1238) was used. The maleic anhydride-grafted HDPE (PE-*g*-MAn, Fusabond MB100D, DuPont Canada) was used as a coupling agent. Organically modified clay with dimethyl dehydrogenated tallow alkyl ammonium (Cloisite 20A, Southern Clay Products) was employed as a layered silicate. A commercial grade carbon dioxide provided by Praxair was utilized as a blowing agent.

3.2. Preparation of HDPE/clay nanocomposites

HDPE/clay nanocomposites were prepared using a parallel counter-rotating intermeshing twin-screw extruder (Model D6/2, C.W. Brabender, diameter = 42 mm, $L/D = 10$) having a barrel temperature profile ranging from 140 to 180 °C from the feeding zone to the die zone. The residence time depends on screw rpm and the characteristics of materials like MFI or viscosity. In this case, the screw speed was set as 70 rpm. HDPE and Cloisite 20A were used as it is without special treatment. Prior to extrusion, organoclay powder, PE-*g*-MAn and HDPE were mixed thoroughly in a container and placed into the hopper of a screw feeder. The PE-*g*-MAn content was fixed at 15 wt% and the clay contents were varied at 0.5, 1.0, and 2.0 wt%. The extrudate was pelletized. The pelletized HDPE/clay nanocomposites were then compression molded with a hydraulic heated press machine (Caver Inc.) for 10 min using 5 ton of force (1.52 MPa). The temperature of the hot pressing plates was 160 °C. The molded samples were quenched in cold water to room temperature. The size of compression-molded samples was 6 mm × 50 mm × 1.55 mm (width × length × thickness).

3.3. Microcellular foaming

A batch microcellular foaming process was used for foaming. In the first stage, the compression-molded samples were saturated in a pressurized CO_2 chamber at 5.8 MPa, at room temperature, for 85 h. Then, the pressure was released rapidly to supersaturate the samples with CO_2. The samples were immersed in a hot glycerin bath for foaming, where the foaming temperature was 130 °C. In order to control the expansion ratio, variable foaming times were used. The foamed samples were immediately quenched in cold water to prevent cell deterioration.

3.4. Sample characterization and mechanical testing

The morphology of HDPE/clay nanocomposites was studied by transmission electron microscopic (TEM) analysis.

Ultra thin sections (70 nm thickness) of the nanocomposite samples were cut by ultracryomicrotome equipped with a diamond knife. Images were recorded using a Hitachi HD-2000 STEM microscope operating at 200 kV. Foam density was measured by a buoyancy method using a density determination kit supplied by Denver Instruments. The Archimedean principle was applied for determining the specific gravity of the foams. The relative foam density is defined as the ratio of the foamed to unfoamed polymer density, whereas the expansion ratio is defined as its inverse. The foam samples were examined using scanning electron microscopy (SEM). The samples were coated using a cold coating process by applying a thin layer of gold with the aid of a sputter coater (SEM Coating Unit PS3). The gas pressure was set at 2 kPa (20 mbar) and the current was applied at 9–10 mA. The entire coating time lasted 70 s. The edges of the coated samples and the SEM mounts were then painted with a conductive carbon paste. A JSM scanning electron microscope (Model 6060) was then operated at 20 kV, and images were acquired from several locations on each sample.

Uniaxial tensile mechanical tests were performed with an Instron 4482 machine with a 100 kN load cell at room temperature. A crosshead speed of 50 mm/min was used, and the strain was measured based on the change in the displacement of the crosshead. The elastic modulus was obtained from the maximum slope at the initial elastic portion of the stress–strain curves. The tensile strength and elongation at break were also reported. A minimum of five specimens was tested for each data point and the averages were reported.

4. Results and discussion

4.1. Characterization

The transmission electron micrographs of HDPE/clay nanocomposites are shown in Fig. 5. To all of three clay loading cases, intercalated clay clusters dispersed in the polymer matrix are detected. As shown in the figure the thickness of intercalated clay clusters is decreased as clay content increases, which means that interlayer spacing in clay clusters is decreased as clay content increases. Fig. 6 shows the scanning electron micrographs of foamed samples. HDPE/clay nanocomposites produced foams of smaller cell size (≈ 1 μm) and also show low foaming grade. This phenomenon is due to low solubility and diffusivity of CO_2 by the crystalline structure in HDPE. In general, compared to the amorphous polymer, foaming of the semicrystalline polymer is difficult because of the crystalline structures in the semicrystalline polymer, which was demonstrated in Refs. [31,33,51,52], where the expansion ratio was decreased with increasing crystallinity. Also, the foaming grade of HDPE is usually decreased with increasing molecular weight or with decreasing melt flow index [53]. With increasing molecular weight, cell size is decreased and cell density is increased [53].

The effects of clay contents and foaming times on the volume expansion ratio of HDPE/clay nanocomposite foams are shown in Fig. 7. The figure indicates that relatively low

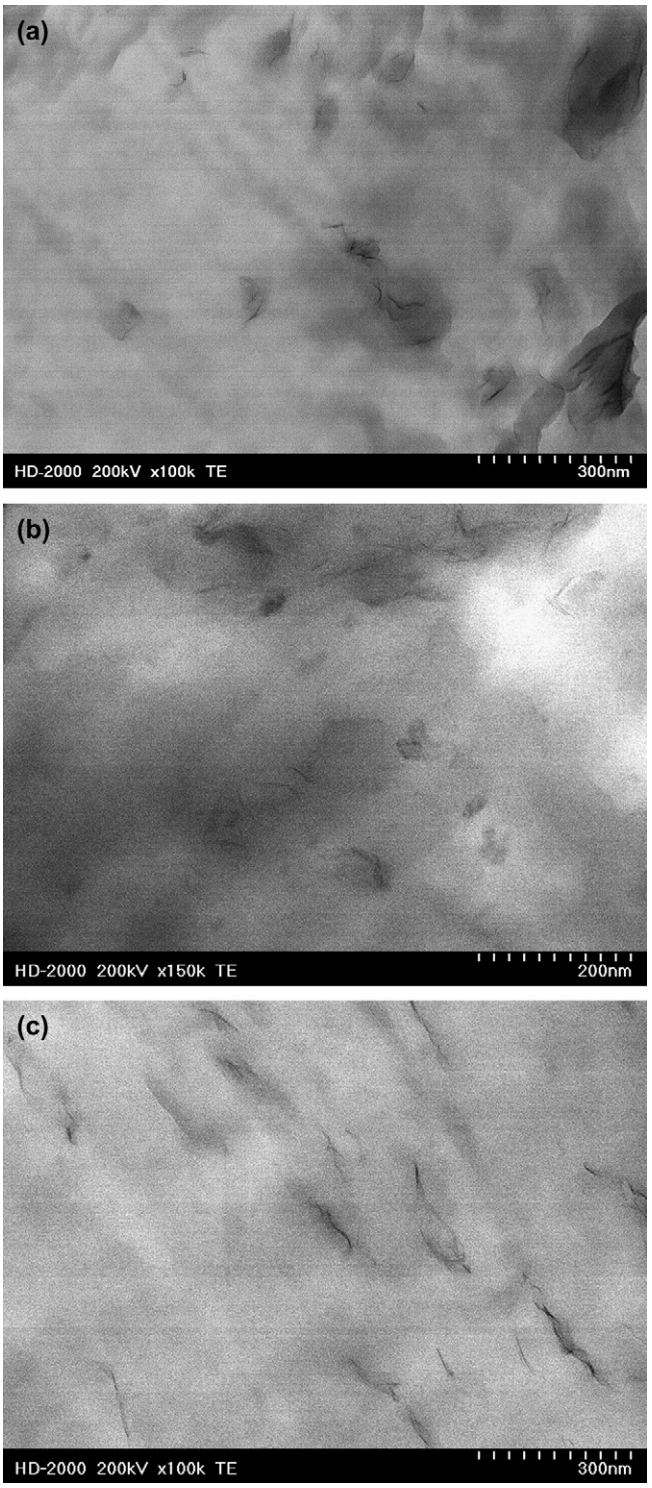

Fig. 5. Transmission electron micrographs of HDPE/clay nanocomposites: (a) 0.5 wt% clay; (b) 1.0 wt% clay; (c) 2.0 wt% clay.

void fractions were achieved. This result is similar to the Rachtanapun's [38] experimental result, where the volume expansion ratios of HDPE foams could reach up to 1.067. From Fig. 7, it was demonstrated that clay particles provide favorable condition for foaming in HDPE. Since the crystallinity decreases with increasing clay contents [54], high clay

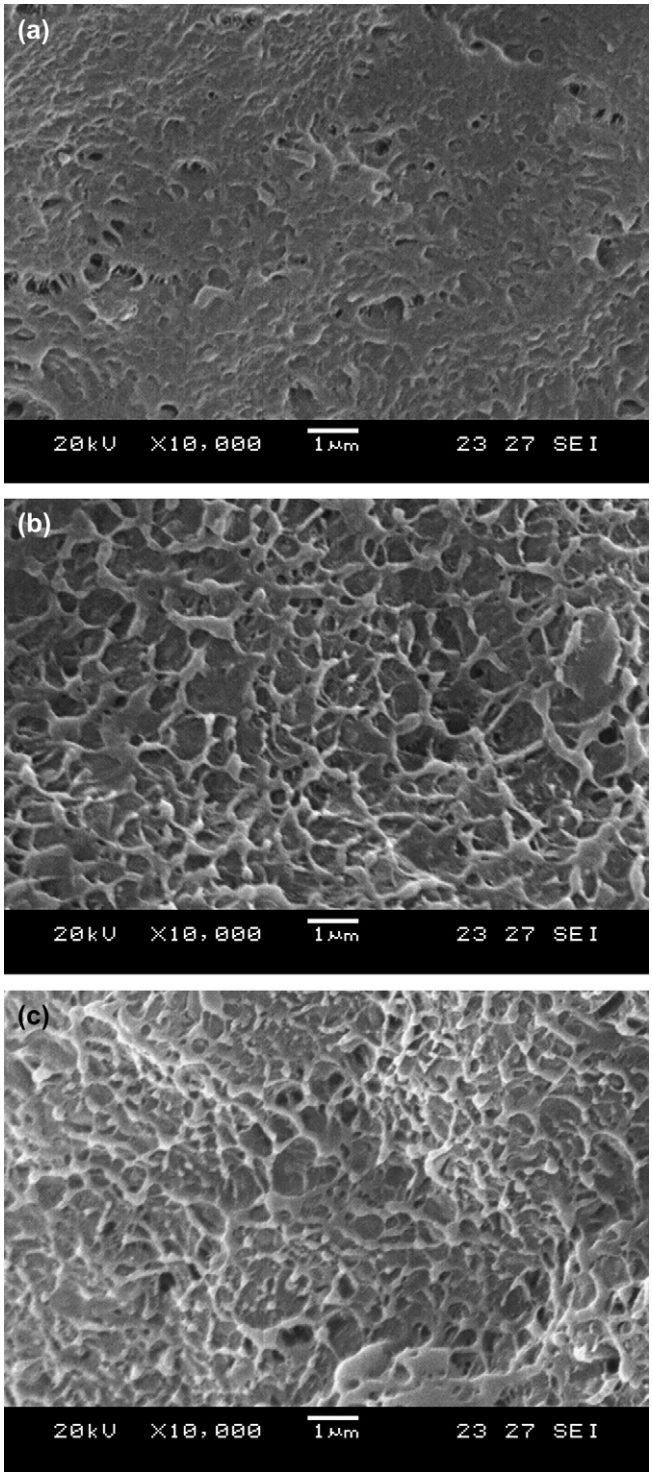

Fig. 6. Scanning electron micrographs of HDPE/clay nanocomposite foams (×10 000): (a) 0.5 wt% clay; (b) 1.0 wt% clay; (c) 2.0 wt% clay.

loadings result in a drop in crystallinity and, consequently, can result in a favorable effect on foaming. Higher volume expansion can be achieved by increasing the foaming temperature [38,39], or by using low-molecular weight HDPE, or lower viscosity material [53]. However, high foaming temperature may cause the deformation of the samples and, as a result, decreases the mechanical strength.

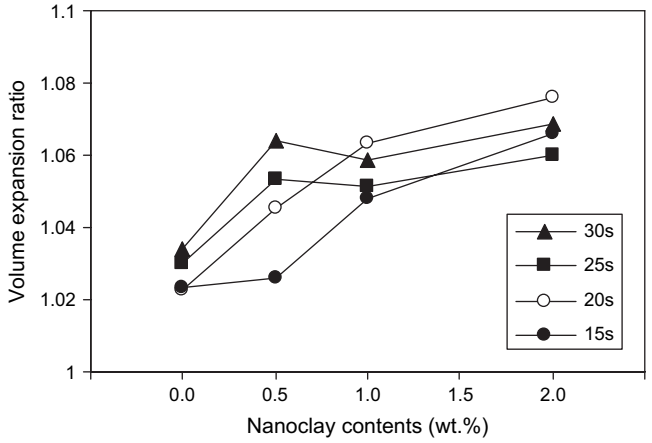

Fig. 7. Effect of clay content and foaming time on the volume expansion ratio of HDPE/clay nanocomposite foams.

4.2. Mechanical properties

Dispersed clay platelets in HDPE led to increased elastic properties, and also resulted in a reduction of the degree of crystallinity [34]. In this experiment, the elastic modulus of HDPE was improved by 9% when nanoclays were added (Fig. 8). However, the variation of the elastic modulus by increasing clay contents was small. This could be a result of the degree of the intercalation. Other researchers reported that the clay fraction in HDPE has little effect on the intercalation extent within 5 wt% clay loadings [17]. In Fig. 8, theoretical prediction was compared with the test results. In the model, $d_m/d_p = 5$, 4, and 3 were used for 0.5, 1.0, and 2.0 wt% clay composites, respectively, which were determined on the basis of XRD studies of HDPE/clay nanocomposites [15,55–57]: When 1.0 and 2.0 wt% clay (Cloisite 20A) concentration was used the d-spacing of the clay was measured as 35 Å [56] and 30 Å [17], respectively, which indicates that macromolecular chains are intercalated into the interlayer of Cloisite 20A. In the case of these interlayer distances, the ratios of clay layer spacing and clay layer thickness (d_m/d_p) for 1.0 and 2.0 wt% clay concentration are calculated as 2.5 and 2, respectively,

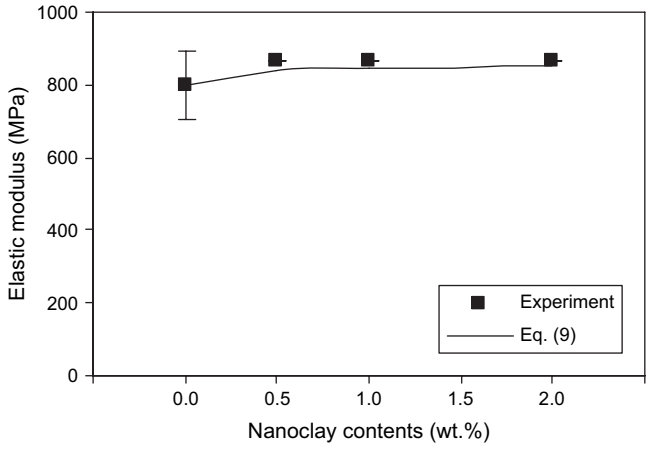

Fig. 8. Effect of clay loading on the elastic modulus of HDPE/clay nanocomposites.

in which 1 nm thick of silicate layers was used [58]. Also, it was reported that the d-spacing of Cloisite 20A was enlarged from 24 Å to 35.6 Å at 2.5 wt% clay concentration [55], which corresponds to $d_m/d_p = 2.6$. No obvious change in clay layer spacing is found for HDPE/clay nanocomposite when the clay content increases from 2 to 5 wt%, however, the d-spacing was proved to be decreased with increasing clay concentration [17,55]. The d-spacing of clays can also be increased by maleic anhydride-grafted polyethylene (PE-g-MAn). When organic-montmorillonite (Org-MMT) is added in HDPE/clay nanocomposites the d-spacing of Org-MMT is increased as the content of PE-g-MAn increases [57]. Thus, in the present model, 1.5 times of d_m/d_p values were adopted as $d_m/d_p = 4$ and 3 for 1.0 and 2.0 wt% clay loadings, respectively, because 15 wt% of maleic anhydride-grafted polyethylenes were used in the HDPE/clay nanocomposites. Also, for the case of 0.5 wt% clay loadings, more increased interlayer spacing of clays ($d_m/d_p = 5$) was used in the model. The number of clay layers (n_p) in each intercalated clay cluster was assumed as 5. As shown in Fig. 8, the developed model for the elastic modulus of HDPE/clay nanocomposites was found to have a trend similar to the experimental results.

The effect of the clay loadings on the elastic modulus of HDPE/clay nanocomposite foams is shown in Fig. 9. The reinforcing effect of the clays on the elastic modulus of foams was maximized when clay loading was 0.5 wt%, and then decreased with increasing clay content. In other words, the rate of decrease of elastic modulus by foaming becomes the least at 0.5 wt% clay loading. This decreasing phenomenon of the relative elastic modulus implies that some of the nanoclays acted to have a deteriorating effect on the foams after 0.5 wt% clay loading. Lee et al. [16] reported that some stacked clays were found above 3 wt% clay loading when PE-g-MAn was used as a compatibilizer in synthesizing nanocomposites. In this case, montmorillonite was treated with a swelling agent (octadecylamine) before melt mixing to increase the interlayer distance of the clays. However, in this study, clays are used as received in the melt compounding. Accordingly, the deteriorating effect by stacked clays might be created before 3 wt% clay loadings in this experiment. The theoretical models for tensile elastic modulus of HDPE/clay nanocomposite foams were compared with the experimental results shown in Fig. 10, where the Poisson's ratio was fixed as 0.35. As shown in the figure, the elastic modulus decreased

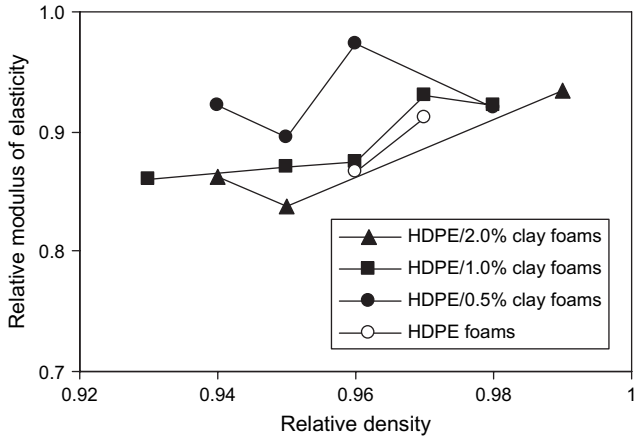

Fig. 9. Effect of clay content on the relative elastic modulus of HDPE/clay nanocomposite foams.

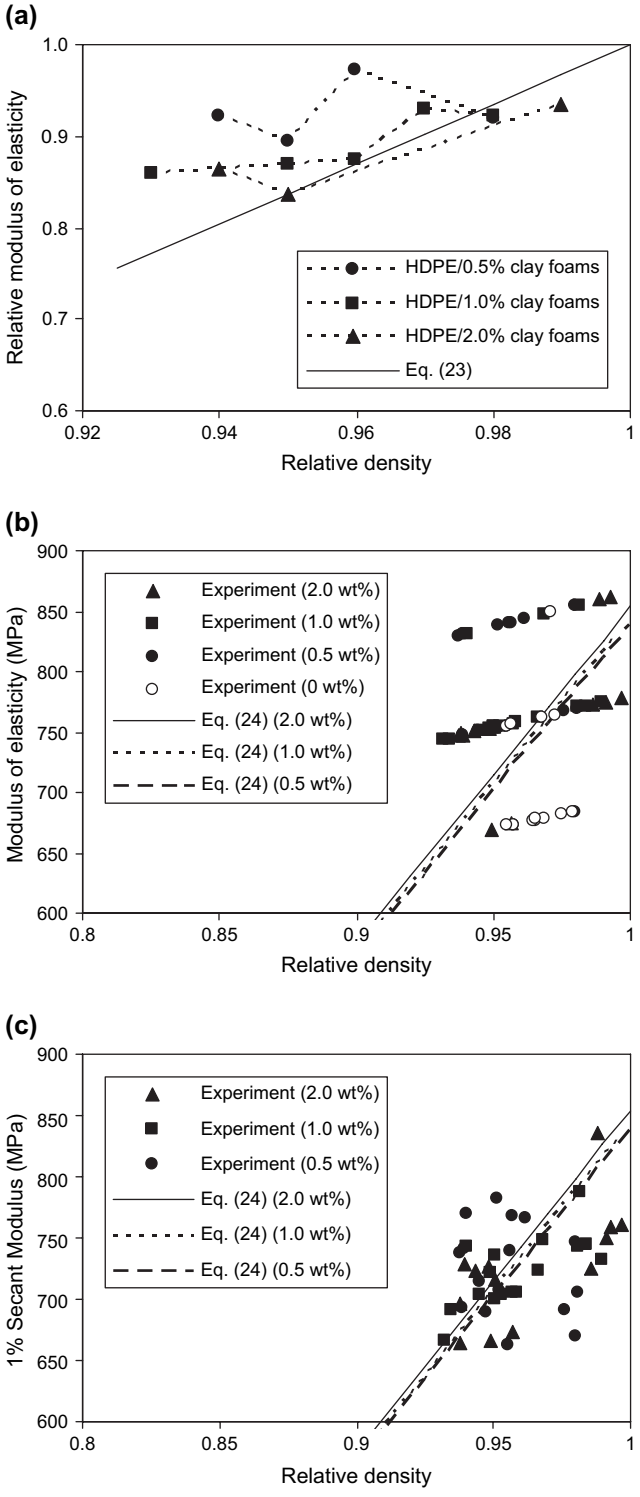

Fig. 10. Comparison of the theoretical prediction for tensile elastic modulus of HDPE/clay nanocomposite foams with experimental results: (a) relative elastic modulus; (b) elastic modulus; (c) 1% secant modulus.

as the relative density decreases. As indicated in Fig. 10a, Eq. (23) is representing the elastic modulus of foams at high relative density. Thus, the application of Eq. (23) in Eq. (24) is regarded as appropriate. The test results of the elastic modulus in Fig. 10b may look as consisted of three data groups, which are due to the limited recording system from the tensile test machine. Also the figure look as there is big deviation between experiment and prediction. However, the elastic modulus decreases with decreasing the relative density because the change in the experimental elastic moduli moves between data groups. Also, the theoretical curves in the figure are connecting the each data group. To compare the theoretical models with experimental results more accurately, 1% secant modulus was used in Fig. 10c. The 1% secant modulus is smaller than the elastic modulus (≈0% secant modulus) used in Fig. 10b by approximately 6.5%. However, the 1% secant modulus can be representative of the tensile modulus in this experiment as it is quite close to the maximum modulus values. Also, the use of the modulus can be an effective method for fully nonlinear elastic behavior as well as it can overcome the limit of the recording system of test machine. As shown in Fig. 10c the theoretical model (Eq. (24)) predicts the tensile elastic modulus well. Also, this model shows no big difference between clay contents as represented by experimental data.

The tensile strength of the HDPE/clay nanocomposite was also improved by 5–7% by adding nanoclays as shown in Fig. 11. When HDPE/clay nanocomposites contain partially intercalated/exfoliated clays, their tensile modulus and tensile strength could increase continuously up to 7 wt% clay loadings [16]. In this study, however, the tensile strength creates no big difference to the change in the clay contents within 2.0 wt% clay loadings and some decreasing phenomenon after 1.0 wt% was found out as well. This implies that some of the clays in the samples remain in the stacked state and resulted in a retrogressive effect on the reinforcing process. Murphy et al. [24] also reported that organoclay loading in polyethylene had an adverse effect on the tensile yield stress. As shown in Fig. 12, the HDPE/clay foams containing 0.5 wt% nanoclay had higher tensile strength than other clay loadings.

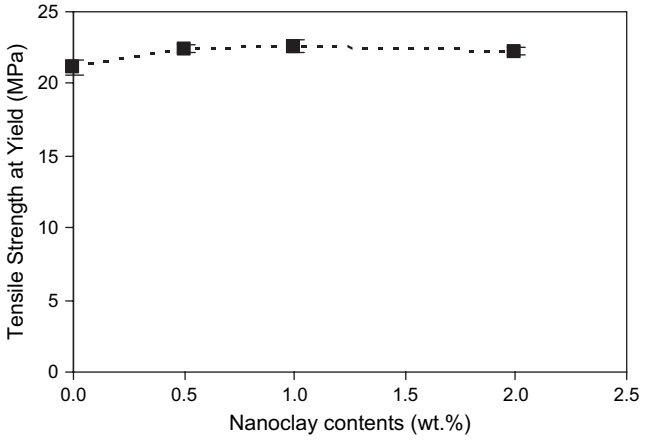

Fig. 11. Effect of clay loadings on the tensile strength of HDPE/clay nanocomposites.

The percent elongation at yield decreased by 20 when nanoclays were added to the HDPE, and the variation was small between 0.5% and 2.0% clay loadings (Fig. 13). The decrease in yield strain is probably due to the confined movement of the polymer between the clay particles. The percent elongation at break of HDPE was considerably reduced with the addition of nanoclays (Fig. 14). As foaming increases, the percent elongation at break decreased until the relative density was 0.95 and

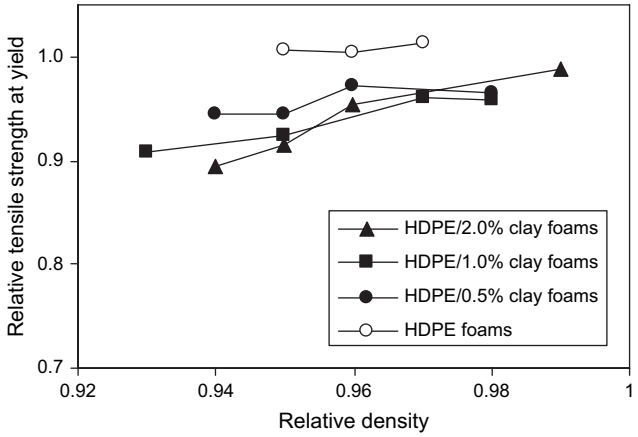

Fig. 12. Effect of clay loadings on the relative tensile strength at yield of HDPE/clay nanocomposite foams.

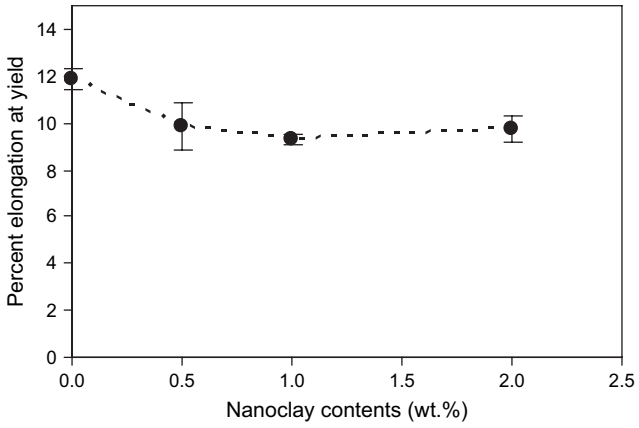

Fig. 13. Percent elongation at yield of HDPE/clay nanocomposites.

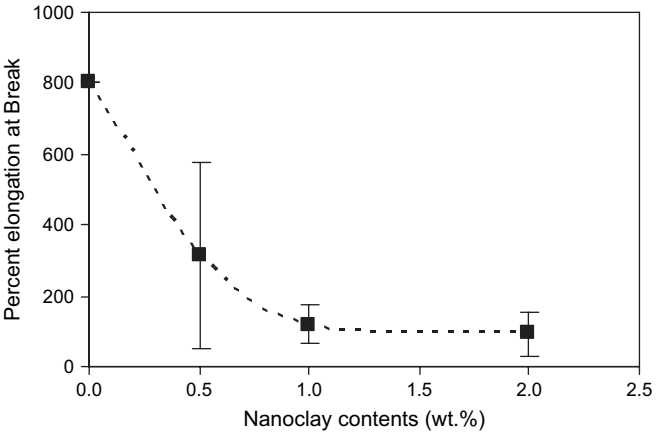

Fig. 14. Percent elongation at break of HDPE/clay nanocomposites.

began to increase again (Fig. 15). Also, the percent elongation at break decreased as the clay content increased. Similarly, as tensile strength, the highest percent elongation of the foams was obtained at 0.5 wt% clay loading.

The uniaxial tensile test results of the HDPE/clay nanocomposites and nanocomposite foams are plotted in Fig. 16. The

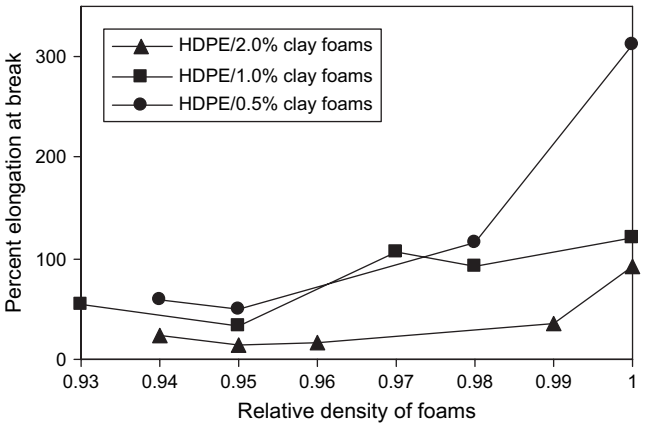

Fig. 15. Percent elongation at break of HDPE/clay nanocomposite foams.

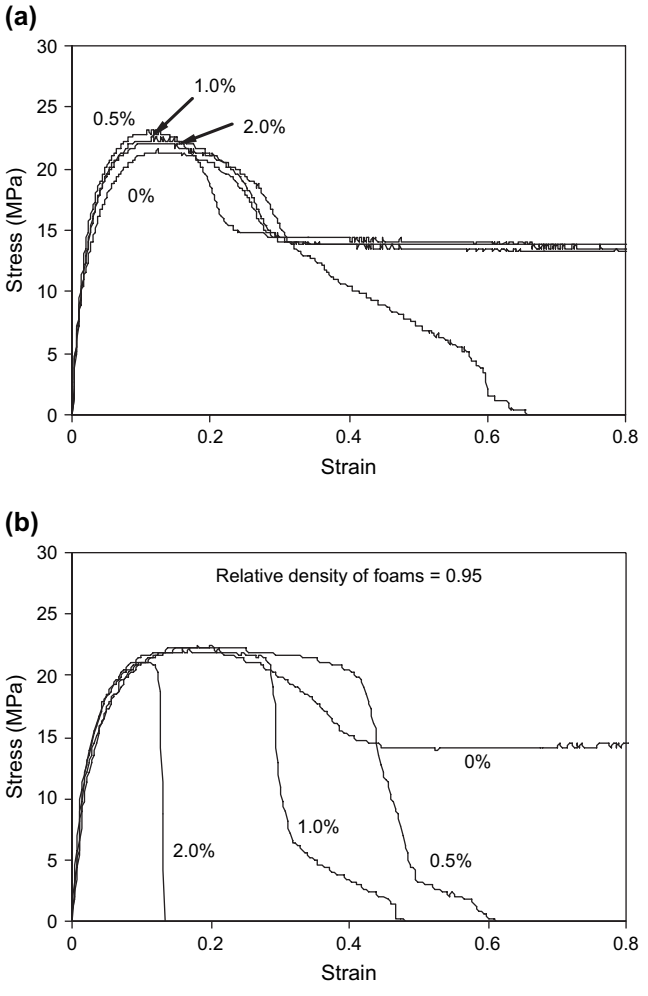

Fig. 16. Effect of clay loadings on the tensile behavior of: (a) HDPE/clay nanocomposites and (b) HDPE/clay nanocomposite foams.

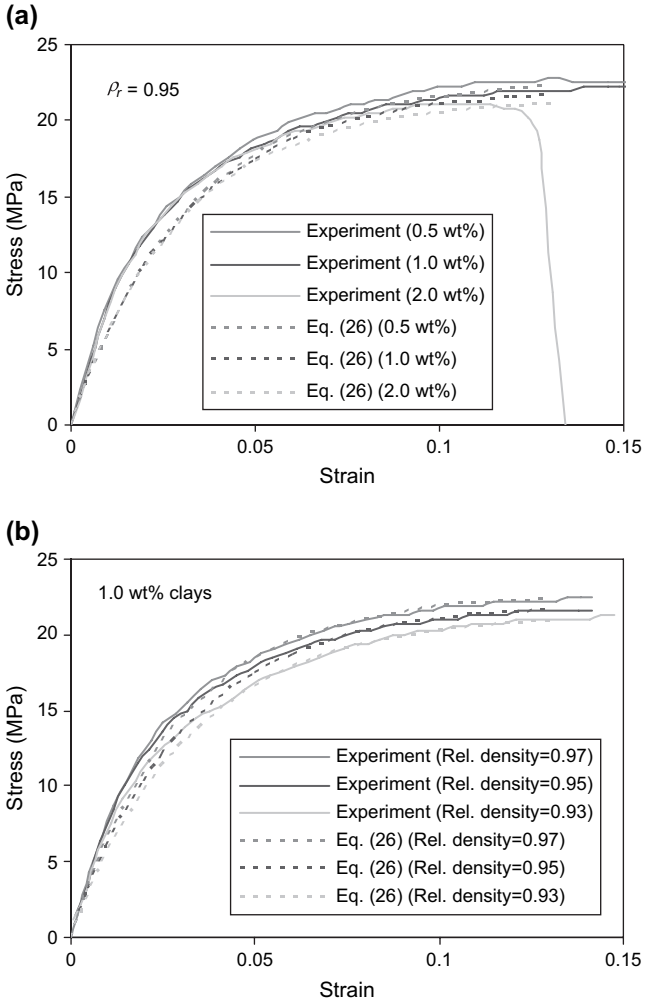

Fig. 17. Tensile elastic behaviors of HDPE/clay nanocomposite foams depending on: (a) the clay contents and (b) the relative densities.

HDPE/clay nanocomposites show plastic deformation resulting from the separation of the crystalline block segments in HDPE. By adding clay particles, the elastic modulus and tensile strength of HDPE were improved somewhat. However, the percent elongation at break decreased greatly as the clay content increased. The percent elongation at yield of HDPE/clay nanocomposites changed a little with clay loading. The proposed constitutive model was compared with experimental results in Fig. 17. The effects of clay contents and relative density of foams on the tensile behavior were investigated with model prediction. The viscoelastic properties of HDPE/clay nanocomposite foams were well described by the model. The viscoplastic model which can be applied after yielding will be studied in the future work.

5. Conclusion

The effects of the nanoclay and foaming conditions on the foam morphology and tensile mechanical properties of polymer/clay nanocomposite foams were studied. The microcellular closed-cell nanocomposite foams were prepared by batch

foaming process with 0.5, 1.0, and 2.0 wt% nanoclay loadings. The effect of clay contents and foaming conditions on the cell morphologies such as cell size and volume expansion ratio, and on the mechanical properties such as elastic modulus, tensile strength, and elongation at break was investigated. The nanoclays in both nanocomposites and nanocomposite foams played a role in improving the mechanical properties such as elastic modulus and tensile strength at yield. Compared to the pure HDPE foams, HDPE/clay foams showed better tensile properties. At 0.5 wt% nanonclay loading, the mechanical properties of both nanocomposites and nanocomposite foams were improved most. A constitutive model for characterizing the tensile elastic behavior of HDPE/clay nanocomposite foams was developed using micromechanics theory and compared with the experimental results. Within high relative density region, the theoretical model could predict the uniaxial tensile elastic behavior of HDPE/clay nanocomposite foams.

References

[1] Giannelis EP. Adv Mater 1996;8:29–35.
[2] Alexandre M, Dubois P. Mater Sci Eng 2000;28:1–63.
[3] Bharadwaj RK. Macromolecules 2001;34:9189–92.
[4] Kumar S, Jog JP, Natarajan U. J Appl Polym Sci 2003;89:1186–94.
[5] Du J, Zhu J, Wilkie CA, Wang J. Polym Degrad Stab 2002;77:377–81.
[6] Manninen A, Naguib HE, Nawaby AV, Xia L, Day M. Cell Polym 2005;24:49–70.
[7] Kumar V, VanderWel M, Weller J, Seeler KA. J Eng Mater Technol 1994;116:439–45.
[8] Klempner D, Frisch KC. Handbook of polymeric foams and foam technology. Munich: Hanser Publishers; 2004.
[9] Matuana LM, Park CB, Balatinecz JJ. Cell Polym 1998;17:1–16.
[10] Collias DI, Baird DG, Borggreve RJM. Polymer 1994;35:3978–83.
[11] Baldwin DF, Suh NP. ANTEC '92, SPE technical paper, vol. 38. 1992. p. 1503–7.
[12] Seeler KA, Kumar V. J Reinf Plast Compos 1993;12:359–76.
[13] Taylor DM, Fernandez O. IEEE Trans Dielectrics Electrical Insulation 2005;12:768–78.
[14] Xiang B, Guan R, Fang Q, Xiao Z, Jiang Y. J Appl Polym Sci 2006; 99:1760–6.
[15] Osman MA, Rupp JEP, Suter UW. Polymer 2005;46:1653–60.
[16] Lee J-H, Jung D, Hong C-E, Rhee KY, Advani SG. Compos Sci Technol 2005;65:1996–2002.
[17] Zhong Y, Kee DD. Polym Eng Sci 2005;45:469–77.
[18] Lee KY, Paul DR. Polymer 2005;46:9064–80.
[19] Luo J-J, Daniel LM. Compos Sci Technol 2003;63:1607–16.
[20] Cho JW, Paul DR. Polymer 2001;42:1083–94.
[21] Lee KY, Goettler LA. Polym Eng Sci 2004;44:1103–11.
[22] Vu YT, Rajan GS, Mark JE, Myers CL. Polym Int 2004;53:1071–7.
[23] Kuo MC. Mater Chem Phys 2005;90:185–95.
[24] Murphy MJ, Truss R, Halley P, Martin D, Ang CL. ANTEC; 2003. p. 1189–93.
[25] Dommelen JAW, Parks DM, Boyce MC, Brekelmans WAM, Baaijens FPT. J Mech Phys Solids 2003;51:519–41.
[26] Dommelen JAW, Schrauwen BAG, Breemen LCA, Govaert LE. J Polym Sci Part B Polym Phys 2004;42:2983–94.
[27] Drozdov AD, Christiansen J. J Appl Polym Sci 2003;88:1438–50.
[28] Sheng N, Boyce MC, Parks DM, Rutledge GC, Abes JI, Cohen RE. Polymer 2004;45:487–506.
[29] Nikolov S, Doghri I, Pierard O, Zealouk L, Goldberg A. J Mech Phys Solids 2002;50:2275–302.
[30] Drozdov AD, Christiansen J. Eur Polym J 2007;43:10–25.
[31] Jo C, Fu J, Naguib HE. Constitutive modeling for intercalated PMMA/clay nanocomposite foams. Polym Eng Sci 2006;46:1787–96.
[32] Schultz JM. Polymer crystallization: the development of crystalline order in thermoplastic polymers. Washington, DC: Oxford University Press; 2001 [chapter 4].
[33] Lee YH, Park CB, Wang KH, Lee MH. J Cell Plast 2005;41:487–502.
[34] Gopakumar TJ, Lee JA, Kontopoulou M, Parent JS. Polymer 2002;43:5483–91.
[35] Yano K, Usuki A, Okada A, Kurauchi T, Kamigaito O. J Polym Sci Part A Polym Chem 1993;31:2493–8.
[36] Usuki A, Koiwai A, Kojima Y, Kawasumi M, Okada A, Kurauchi T, et al. J Appl Polym Sci 1995;55:119–23.
[37] Ji XL, Jing JK, Jiang W, Jiang BZ. Polym Eng Sci 2002;42:983–93.
[38] Rachtanapun P, Selke SEM, Matuana LM. J Appl Polym Sci 2003; 88:2842–50.
[39] Rachtanapun P, Selke SEM, Matuana LM. J Appl Polym Sci 2004; 93:364–71.
[40] Nemat-Nasser S, Hori M. Micromechanics: overall properties of heterogeneous materials. North-Holland; 1993.
[41] Li ZR, Lim CW, He LH. Eur J Mech A Solids 2006;25:260–70.
[42] Lubarda VA, Richmond O. Mech Mater 1999;31:1–8.
[43] Yin HP, Ehrlacher A. Mech Mater 1996;23:287–94.
[44] Krstic VD. Acta Metall 1985;33:521–6.
[45] Molinari A, Canova GR, Ahzi S. Acta Metall 1987;35(12):2983–94.
[46] Lin L, Argon AS. J Mater Sci 1994;29:294–323.
[47] Bartczak Z, Argon AS, Cohen RE. Macromolecules 1992;25(19): 5036–53.
[48] Bartczak Z, Cohen RE, Argon AS. Macromolecules 1992;25(18): 4692–704.
[49] Nikolov S, Doghri I. Polymer 2000;41:1883–91.
[50] Jo C, Fu J, Naguib HE. Polymer 2005;46:11896–903.
[51] Doroudiani S, Park CB, Kortschot MT. Polym Eng Sci 1996;36: 2645–62.
[52] Doroudiani S, Park CB, Kortschot MT. Polym Eng Sci 1998;38:1205–15.
[53] Zhang Y, Rodrigue D, Ait-Kadi A. J Appl Polym Sci 2003;90:2111–9.
[54] Min KD, Kim MY, Choi K-Y, Lee JH, Lee S-G. Polym Bull 2006; 57:101–8.
[55] Swain SK, Isayev AI. Polymer 2007;48:281–9.
[56] Tzavalas S, Macchiarola K, Gregoriou VG. J Polym Sci Part B Polym Phys 2006;44:914–24.
[57] Liang G, Xu J, Bao S, Xu W. J Appl Polym Sci 2004;91:3974–80.
[58] Giannelis EP, Krishnamoorti R, Manias E. Adv Polym Sci 1999; 138:107–47.